Journal of Materials Chemistry C

Accepted Manuscript

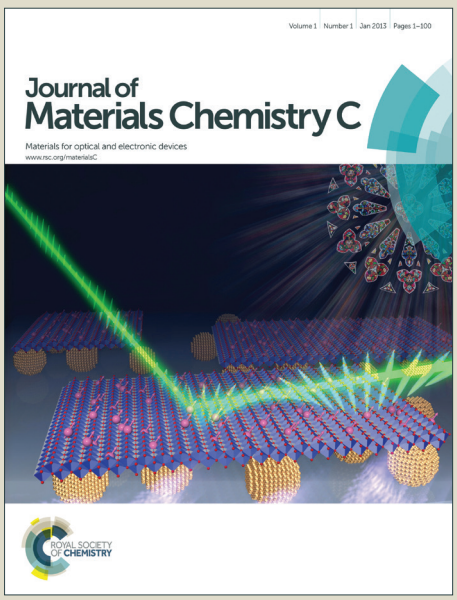

ROYAL SOCIETY OF CHEMISTRY

www.rsc.org/materialsC

Journal of Materials Chemistry C RSCPublishing

ARTICLE

Yolk-shell Fe_3O_4@ZrO_2 prepared by a tunable polymer surfactant assisted sol-gel method for high temperature stable microwave absorption

Cite this: DOI: 10.1039/x0xx00000x

Received 00th January 2012,
Accepted 00th January 2012

DOI: 10.1039/x0xx00000x

www.rsc.org/

Meng Yu[a] Chongyun Liang[c] Mengmei Liu[b] Xialin Liu[a] Kaiping Yuan[a] Hui Cao[a] and Renchao Che[a,b]

Highly-dispersed Fe_3O_4@ZrO_2 yolk-shell structures with ZrO_2 shell of homogeneous shell thickness is successfully prepared via a polymer surfactant (hydroxypropyl cellulose) assisted sol-gel method. By using HPC as a surfactant, high dispersed particles with Zirconia shell of about 25-30nm in thickness was obtained. The yolk-shell Fe_3O_4@ZrO_2 structure is characterized by combined techniques including transmission electron microscopy (TEM), scanning electron microscopy (SEM) and X-ray diffraction (XRD) indicating the particle has a ZrO_2 shell of 500 nm in diameter, 25-30 nm in thickness and a Fe_3O_4 core of 300 nm in diameter. An *in-situ* TEM heating experiment from 20 ºC to 1000 ºC demonstrates the obtained yolk-shell Fe_3O_4@ZrO_2 structure is stable without any distinguished structural damage below 700 ºC. This material has great potential in acting as a high temperature stable microwave absorber. Even under the temperature of 500 °C, this material still preserved over 90% of the reflection loss (RL) value compared with the room temperature property. These findings may shed light on the development of novel microwave absorber working under high temperature.

Introduction

Recently, yolk-shell structures have attracted considerable attention in a wide range of applications including nanoreactors[1, 2], catalysis[3-5], drug delivery[2, 6, 7], lithium-ion batteries[8-10], microwave absorption[11, 12] and biomedical fields[6, 13-15]. The unique structural feature of yolk-shell material is the hollow cavity sandwiched between core and shell, which endows it abundant of tunable chemical properties. ZrO_2 ceramic has many important applications such as catalyst carrier and thermal barrier, due to its chemical inertness, low thermal conductivity and structure stability under high temperature. Hence, lots of work has been done to prepare ZrO_2 based composite structures to improve the thermostability of traditional functional materials[16-18]. The excellent thermostable property of ZrO_2 makes it a promising candidate for yolk-shell structures as it may protect the internal cores under high-temperature. However, to the best of our knowledge, very limited work has been reported previously[19].

Previously, considerable efforts have been paid and several synthetic routes have been proposed for the synthesis of core@ZrO_2 structures[20-27]. For example, Matijevic and co-workers successfully deposited ZrO_2 on polystyrene (PS) spheres based on a heterocoagulation process[26]. Qian and co-workers prepared ZrO_2/PS core-shell microspheres through a combined room-temperature aging and solvothermal process with ethanol as a solvent[25]. Tang and co-workers developed a procedure based on a two-step nanocasting route to prepare monodisperse mesoporous ZrO_2 spheres with high surface area and tailored compositions[22]. Nevertheless, many recently reported works chose microspheres with a SiO_2 surface as the core and the coating reaction of ZrO_2 were based on a sol-gel process, the reason of which is that the development of Stöber method enables us to prepare different kinds of core@SiO_2 structures[28-30], which provides plenty of possibilities to synthesize ZrO_2 shelled yolk-shell structures with different core materials. Kim and coworkers obtained SiO_2@ZrO_2 particles *via* a sol-gel process under 80°C in a H_2O/ethanol solution and studied the mechanism of the reaction[27]. Schüth and coworkers introduced a facile method of surfactant (Lutensol-AO5) assisted sol-gel process to obtain SiO_2@ZrO_2 particles with uniform ZrO_2 layers, furthermore, they successfully prepared yolk-shell Au@ZrO_2 microspheres by etching out the SiO_2 layer of Au@SiO_2@ZrO_2 with NaOH[19, 20]. Although the sol-gel method mentioned above shows its advantages of facile, general and tunable in preparing SiO_2@ZrO_2 structures, there still exist difficulties in obtaining SiO_2@ZrO_2 structures with both high degree of dispersion and tunable shell thickness. The main reasons may be the low electronegativity and the high

coordination numbers of zirconium, which endow its precursors with great reactivity, thus makes it difficult to control the hydrolysis and condensation process which is the dominate factor during a typical sol-gel reaction[31].

As reported previously, several methods were adopted to decrease the hydrolysis rate of the metal precursor in the reaction of coating metal oxide *via* sol-gel method, for examples, low temperature, capping agents, precursors with lower reactivity, mixed solvent[31-33]. All the methods mentioned above are in the consideration of no more than reducing the reactivity of the precursors, or reducing the interaction between precursors and water. Using low temperature or less reactive precursors with are obviously the former type. Choosing capping agents or using mixed solvent are both in the consideration of weakening the interaction between the precursors and H_2O. With the change in alkyl-group on the metal precursors (usually are alkoxide precursors), such as increasing chain length or branching in the alkyl-group of the alkoxide precursors, the solubility of the precursors in water decrease, therefore weakens the interaction between them. Choosing proper mixed solvent also controls the solubility of the precursor in the solvent, thus weakens the interaction[32]. Considering all the factors mentioned above, polymer surfactant might play important role in controlling the hydrolysis of zirconium precursor in a sol-gel process.

Composite structures including yolk-shell structure have become an important developing direction in the study of the microwave absorber nowadays, due to it combined functionalities of cores and shells that endow the absorber broader frequency band, smaller density and stronger absorption. For example, carbon/3d metal (Fe, Ni, Co) nano-composite was prepared for the enhancement in microwave absorption properties[34, 35]. Ferrite@dielectric-metal-oxide was prepared for microwave absorption enhancement within wide frequency range, our group has successfully prepared a series of core-shell and yolk-shell structure materials, $Fe_3O_4@TiO_2$[12, 36]. $Fe_3O_4@SnO_2$[37] and Fe_3O_4@BS/BTO[38] to extend the microwave absorption property of Fe_3O_4 core. However, previous researches on high-temperature stable electromagnetic microwave (EM) absorber were limited due to the difficulties in finding merits of both strong absorption capability and heat resistance from one individual material. Most of the traditional high-temperature stable EM absorbers are the dielectric ceramic materials which have no magnetic loss capability, such as Si-N-C ceramic powder, Al_2O_3 ceramic, BeO ceramic and BN ceramic[39-42]. The magnetic ferrites although have the advantages of strong absorption and wide frequency band over those dielectric ceramics, great difficulty still need to be overcome for their application of high temperature stable absorbers, because ferrites were easily to be oxidized under high temperature. Hence, the yolk-shell $Fe_3O_4@ZrO_2$ (ferrite@ceramic) structural material might have great potential in solving this problem and serving as a high-temperature stable EM absorber as it may combine the thermostability of the ceramic and the microwave absorption property of the ferrite. Nevertheless, ferrite@ceramic absorber working under high-temperature has not been reported until now.

Herein, uniform yolk-shell $Fe_3O_4@ZrO_2$ microspheres were successfully prepared by a HPC-assisted sol-gel process. The thermostability of the material was investigated by an *in-situ* heating TEM experiment at a temperature range from 20 °C to 1000 °C, which reveals that the particle is thermostable under the temperature of 700 °C, higher temperature result in a hollowing transformation of the Fe_3O_4 cores and a crystalline phase change of the ZrO_2 shell. The high-temperature microwave absorption property of the material was evaluated by investigating the microwave absorption property of a series of materials at the temperatures of 20 °C, 250 °C and 500 °C. The results indicated that thick and compact shell protect the cores well at high temperature, whereas the thin and loose shells can only achieve that at 250°C, as higher temperature will cause the loss of magnetism of the material and lead to the decrease of the microwave absorption property.

Results and discussion

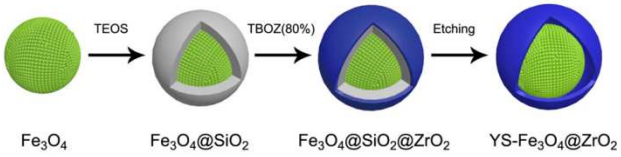

Scheme 1 The schematic illustration of the synthesis procedure in preparing YS(yolk-shell) $Fe_3O_4@ZrO_2$ microspheres.

The procedure of synthesizing yolk-shell $Fe_3O_4@ZrO_2$ particles is consisted of three main steps, as illustrated in Scheme 1. Step 1, uniform Fe_3O_4 microspheres with an average particle size of about 300 nm were prepared by a solvothermal reaction and coated with SiO_2 shells with average thickness of about 60 nm-70 nm by Stöber method afterwards to obtain $Fe_3O_4@SiO_2$ particles. Step 2, ZrO_2 generated by the hydrolysis of zirconium (IV) n-butoxide (TBOZ) in a polymer surfactant (HPC) assisted sol-gel process was deposited on the surface of $Fe_3O_4@SiO_2$ particles to form an amorphous ZrO_2 shell, in which the hydrolysis rate of the zirconium precursor was successfully controlled by introducing proper amount of HPC and H_2O in the reaction system. Step 3, the SiO_2 layer of the $Fe_3O_4@SiO_2@ZrO_2$ particles was removed by treating the particles with 0.5M NaOH solution at 60 °C to get yolk-shell $Fe_3O_4@ZrO_2$ microspheres. Then the product was calcinated at 500 °C in N_2 atmosphere to obtain ZrO_2 shells with good crystallinity.

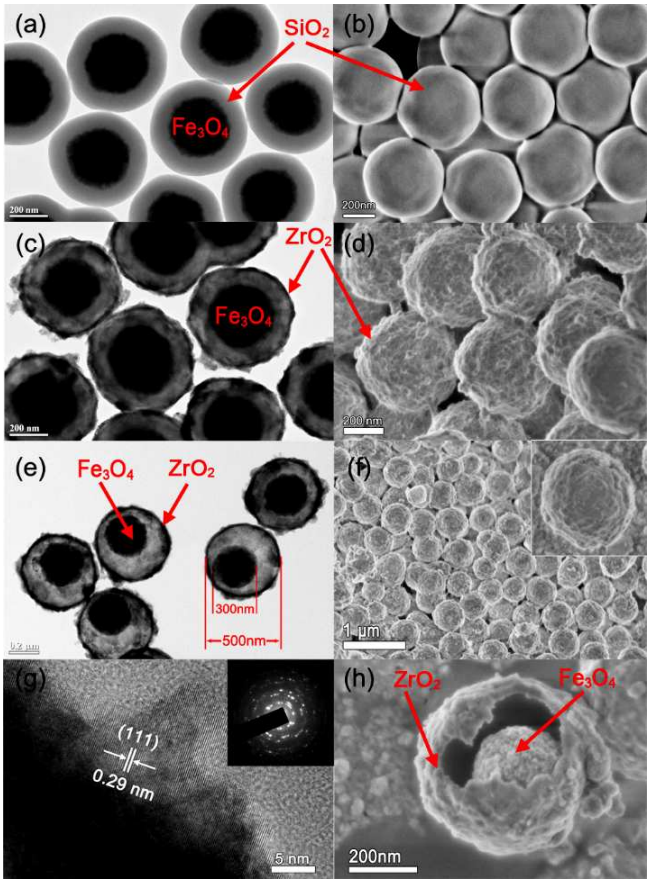

Figure 1 TEM and FESEM images of the (a) and (b) Fe_3O_4@SiO_2, (c) and (d) Fe_3O_4@SiO_2@ZrO_2 microspheres, (e) and (f, h) yolk-shell Fe_3O_4@ZrO_2 microspheres. (g) The SAED pattern and HRTEM image of the particle.

Representative transmission electron microscope (TEM) and field-emission scanning electron microscope (FESEM) images of Fe_3O_4@SiO_2 (Fig 1(a, b)) exhibit uniform core-shell microspheres with cores of 300 nm in diameter and shells of 60-70 nm in thickness, the microspheres own smooth surface (Fig 1(b)) due to the slow and even deposition of SiO_2 on the cores. Fe_3O_4@SiO_2@ZrO_2 microspheres have high dispersibility and integrated ZrO_2 shells (Fig 1(c, d)), with an average particle size of about 500 nm and a ZrO_2 shell thickness of about 25-30 nm. The as-synthesized Fe_3O_4@SiO_2 @ZrO_2 particles exhibited rough surface due to the deposition and growth of ZrO_2 (Fig 1(d)). A procedure of etching SiO_2 was carried out to obtain yolk-shell Fe_3O_4@ZrO_2 microspheres. After the treatment of 0.5M NaOH solution, the SiO_2 was removed through etching without damaging the structure of ZrO_2 shells and Fe_3O_4 cores, leaving a large cavity between the ZrO_2 layer and the Fe_3O_4 core. The characterization to the structure of the yolk-shell Fe_3O_4@ZrO_2 microspheres with high resolution transmission electron microscopy(HRTEM), SEM, and selected area electron diffraction (SAED) (Fig 1(e, f, g, h)) revealed that yolk–shell structure is composed of a moveable Fe_3O_4 core encapsulated inside a well-defined ZrO_2 (Fig 1(h)) shell of about 500 nm in diameter and about 30 nm in thickness (Fig 1(e)). From the SEM image of a broken sphere (Fig 1(h)), a typical yolk-shell structure can be found with a large void between the moveable Fe_3O_4 core and the ZrO_2 shell. After the calcination at 500 °C in N_2 atmosphere, the ZrO_2 shell exhibits good crystallinity (Fig 1(g), and Fig 4(c)). The inter-planar spacing is about 0.299 nm, which corresponds to the (111) plane of cubic phase ZrO_2. Selected area electron diffraction (SAED) pattern of the microsphere also shown the good crystallinity of ZrO_2 and Fe_3O_4 and can be indexed to the cubic phase of ZrO_2 (PDF#49-1642) (Fig 1(g) inset).

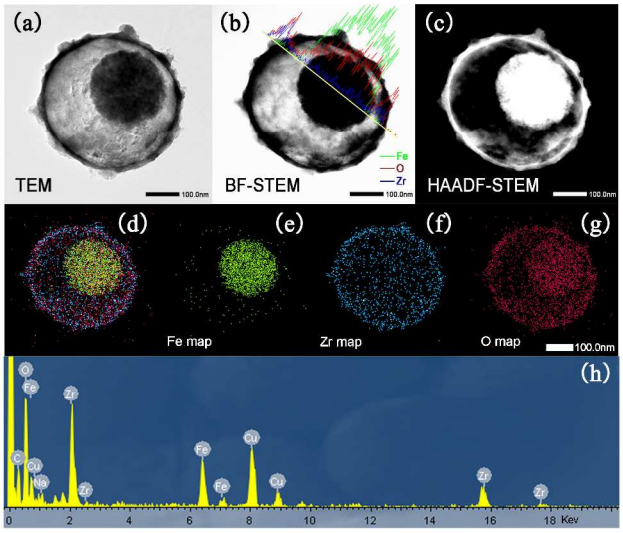

Figure 2 (a), (b) and (c) TEM, BF-STEM and HAADF-STEM images of a typical yolk-shell structure Fe_3O_4@ZrO_2 particle. Line scanning profiles of Fe, Zr and O recorded along the line shown in (b) inset; units for y axis: counts [a.u.]. (d) Combined map, (e) Fe, (f) Zr and (g) O maps. (h) Energy-dispersive X-ray spectroscopy (EDS) analysis of the particle.

Further characterization to the structure of yolk-shell Fe_3O_4@ZrO_2 particles were carried out by high angular annular dark field scanning transmission electron microscopy (HAADF-STEM) and energy dispersive X-ray spectrum (EDS), TEM, bright field scanning transmission electron microscopy (BF-STEM) and HAADF-STEM images of a single particle shows the same yolk-shell structure of the microsphere (Fig 2(a, b, c)). A line scanning profiles of Fe, Zr, and O recorded along the line in Fig 2(b) illustrate that Zr signal are stronger when the line passes through the edge of the shell, Fe signal is stronger when the line passes through the core area of the particle, and O signal is stronger when the line passes through both the edge of the shell and the core area. That provides further evidence for the yolk-shell structure of the microsphere. The corresponding merged map and elemental maps of Fe, Zr and O (Fig 2(d, e, f, g)) demonstrate the actual distributions of Fe, Zr, and O elements separately which match the result of the former characterization perfectly. Combining with those former SEM, TEM, HRTEM, SAED, EDS and XRD characterizations

it can be confirmed that the yolk-shell structural Fe_3O_4@ZrO_2 have been successfully synthesized *via* our synthesis routine.

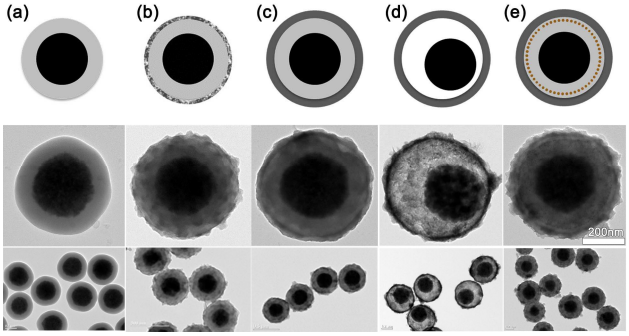

Figure 3. the sketch maps and TEM images of the 5 absorbers, (A) Fe_3O_4@SiO_2 (MA-1), (B) Fe_3O_4@SiO_2@ZrO_2(MA-2) with thin and unintegrated ZrO_2 shells, (C) Fe_3O_4@SiO_2@ZrO_2 (MA-3) with thick and integrated ZrO_2 shells, (D) Fe_3O_4@ZrO_2 (MA-4)with integrated ZrO_2 shells, (E) Fe_3O_4@SiO_2@ZrO_2 with Au nanoparticles dispersed between ZrO_2 shells and SiO_2 shells(MA-5)

Based on this synthesis method, a series of materials can be prepared for the subsequent study of high-temperature microwave absorption property (Fig 3). Fig 3(a) shows the Fe_3O_4@SiO_2 core-shell microspheres (denoted as MA-1) with a Fe_3O_4 core (about 300 nm in diameter) and SiO_2 shell (about 100 nm in thickness). Fig 3(b) are images of the Fe_3O_4@SiO_2@ZrO_2 microspheres with thin and loose ZrO_2 shells (denoted as MA-2) which can be easily prepared by coating MA-1 with ZrO_2 shells, and the shell thickness (about 10 nm) was tuned by simply varying the reaction temperature. Fig 3(c) are images of the Fe_3O_4@SiO_2@ZrO_2 microspheres with thick and compact ZrO_2 shells obtained by coating MA-1 with ZrO_2 shells under room temperature (denoted as MA-3), and the ZrO_2 shell thickness was about 30 nm. Fig 3(d) shows the yolk-shell Fe_3O_4@ZrO_2 microspheres with integrated ZrO_2 shells (denoted as MA-4), which were prepared by etching the SiO_2 layer out of MA-3. Moreover, MA-5 (Fig 3(e)) can be prepared by implanting some gold nanoparticles inside SiO_2 layer before coating ZrO_2 shells. More details for the preparation of MA-5 are provided in supporting information.

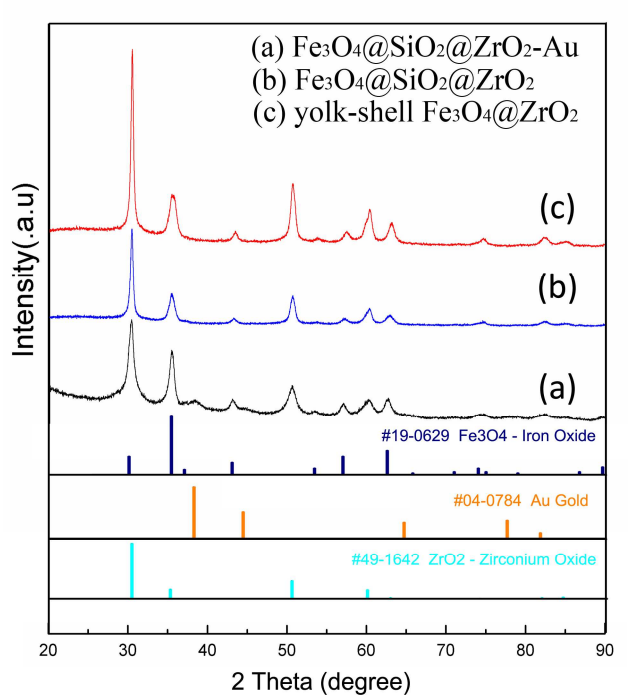

Figure 4 XRD patterns of the Fe_3O_4@SiO_2@ZrO_2-Au microspheres (a), Fe_3O_4@SiO_2@ZrO_2 after calcination at 500°C (b), and yolk-shell Fe_3O_4@ZrO_2 microspheres(c)

The phase purity of these products was evaluated by XRD, The XRD patterns of Fe_3O_4@SiO_2@ZrO_2, Fe_3O_4@ZrO_2, Fe_3O_4@SiO_2@ZrO_2 with Au nanoparticles dispersed between ZrO_2 shells and SiO_2 shells are obtained respectively (Fig 4 (a, b, c)), and match those of Fe_3O_4, ZrO_2 and Au from standard JCPDS (Joint Committee on Powder Diffraction Standards) card PDF#19-0629, PDF#04-0784 and PDF#49-1642 perfectly. No characteristic peaks of other substances were observed in the patterns suggests that no further reaction occurred among the three constituents in Fe_3O_4@SiO_2@ZrO_2 particles in the calcination process at 500 °C besides the crystallization of ZrO_2. Furthermore, the roles played by HPC in the reaction were emphasized as follows.

Table 1 The experimental parameters of group H (H-(1-5)) and group V (V-(1-5)).

Sample	H_2O (mL)	HPC (g)
H-1	0.125	0
H-2	0.125	0.002
H-3	0.125	0.005-0.008
H-4	0.125	0.02
H-5	0.125	0.1
V-1	0.01	0.005
V-2	0.05	0.005
V-3	0.1-0.15	0.005
V-4	0.25	0.005
V-5	0.36	0.005

Two groups of experiments (group H and group V) were designed and carried out to study the dependency of the sol-gel process on the ratio and amount of H_2O/HPC added in the system. In the group H, the H_2O amount as well as the rest parameters of the reaction remained constant, whereas the HPC amount varies at a range from 0 to 0.1 g. In the group V, the amount of HPC and the rest parameters of the reaction remained constant, whereas the amount of H_2O varies at a range from 0.01 mL to 0.36 mL. The parameters of group H and V are shown in Table 1. The samples in the two groups are numbered H-(1-5) and V-(1-5). The results of group H were shown in Fig 5(j, h, f, d, b).The results group V were shown in Fig 5(i, g, e, c, a). According to the result of the experiments. The optimized ZrO2 coating can be obtained while a proper ratio of HPC/H_2O was used in the solution (Fig 5). In the group

H, with the increasing of HPC amount, the quality of ZrO_2 layer increased at the beginning. However, when the HPC amount was larger than 0.008g, the thickness of ZrO_2 shell started to decrease with the increasing of HPC amount. Similarly, in the group V, with increasing of H_2O amount, the thickness of the ZrO_2 layer increased as well. When the amount of H_2O is larger than a value of 0.15mL, the thickness of ZrO_2 decreased with the increasing of H_2O amount. Therefore a proper ratio of HPC/H_2O was essential for this sol-gel process.

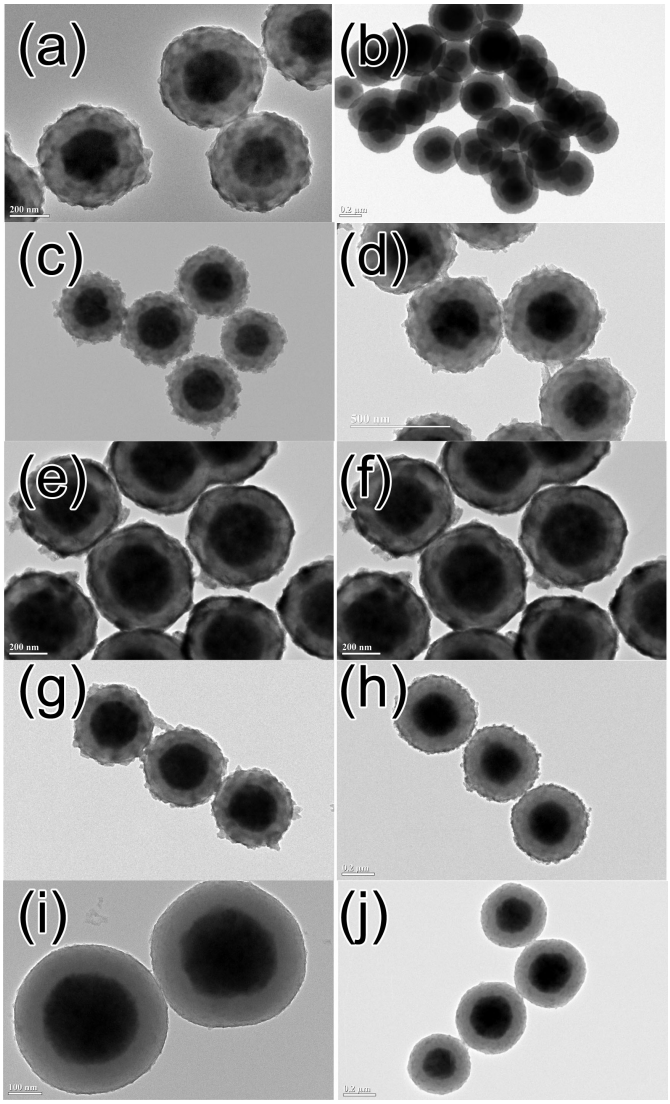

Figure 5 TEM images of the experiment results of group V and H.

An *in-situ* TEM heating experiment was carried out to evaluate the thermostability of the Fe_3O_4@SiO_2@ZrO_2 microspheres (Fig 6). When the temperature was lower than 700 °C, the microspheres didn't show any distinguished structural change (Fig 6(a, b, c)). However, higher temperature led to a hollowing transformation of the internal Fe_3O_4 core (Fig 6(d, e, f)), which might be an inside-out Ostwald ripening process of the core or some reaction between SiO_2 and Fe_3O_4 might have happened. Then we turned the temperature back to room temperature again, and the microsphere with a hollow Fe_3O_4 core can be observed (inset Fig 6h).

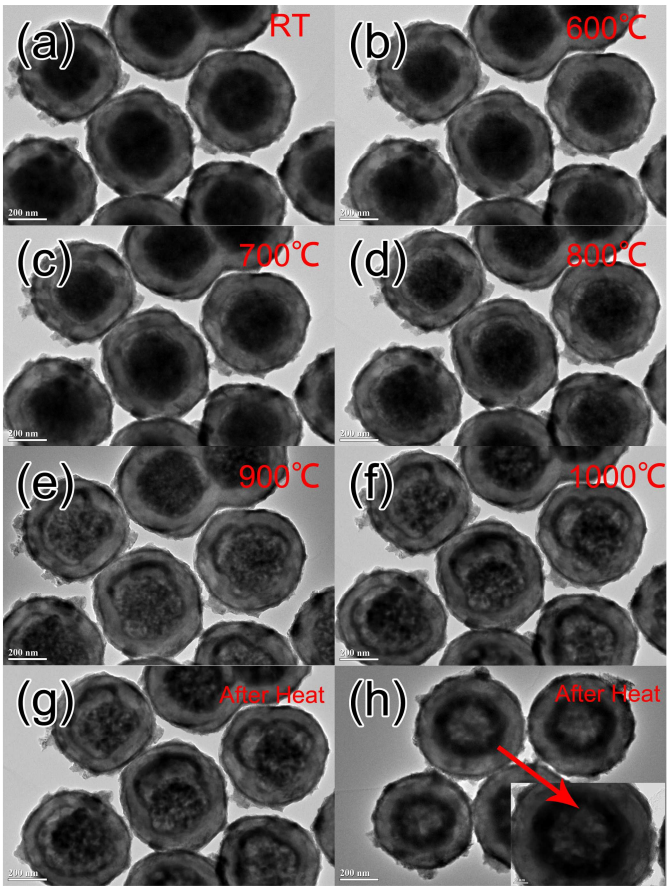

Figure 6 TEM images of the Fe_3O_4@SiO_2@ZrO_2 microspheres under room temperature (a), 600 °C (b), 700 °C (c), 800 °C (d), 900 °C (e), 1000 °C (f), and the images of particles when temperature was turned from 1000°C back to room temperature (g,h).

Fig 7 illustrates the permeability under three temperatures (20 °C, 250 °C, 500 °C measured from those five microwave absorbers mentioned above (MA-1-5). We chose four typical testing frequencies, 3GHz, 8GHz, 13GHz and 18GHz to study the dependency of the electromagnetic parameters on the temperature. The real and imaginary part of complex permeability (μ' and μ'') of MA-1 which represent the magnetic loss property of a absorber went down drastically as the temperature increasing, mainly due to the lacking of protection from ZrO_2 shells (Fig 7). At the temperature of 250°C, μ' and μ'' decreased to 85.2% and 80.5% of the original value comparing with room temperature. While the measured temperature reach 500 °C, μ' and μ'' decreased to 66.7% and 63.3% comparing with that of room temperature. As for MA-2, which owns thin and loose ZrO_2 shells, could in certain degree resist the damage effect with the temperature increasing. However, under higher temperature ZrO_2 can no longer maintain the magnetic property of the materials due to the oxidation of Fe_3O_4 core. When the temperatures increased from

20 °C to 250 °C, the value of μ' and μ'' of the material drop slightly, 94.6% of the μ' value and 94.8% of the μ'' value

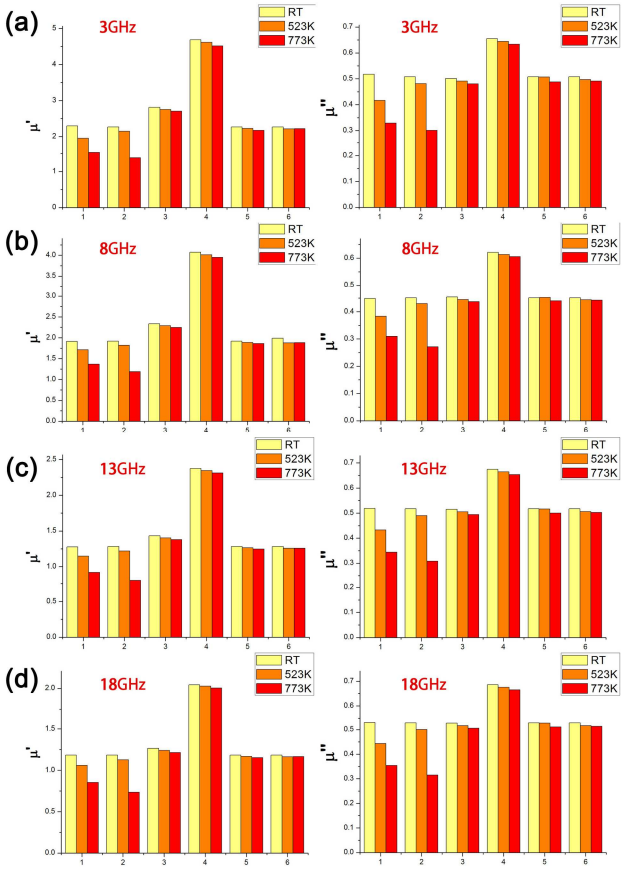

remained. In contrast, when temperature increased from 250°C to 500 °C, the value of μ' and μ'' decreases by a large amount, only 60.9% of μ' and 59.3% of μ'' value remained. It reveals that the thin and loose shells of ZrO_2 can protect the magnetic cores of the materials from being oxidized in some degree; however when the temperature gets higher, the shell is not compact enough to effectively protect the magnetic cores from oxidation. Under a lower temperature (250 °C), the oxidation of the magnetic cores can still be largely avoided even though the ZrO_2 shell not compact enough because the rate of O_2 diffusion was gentle. However, under a higher temperature (500 °C), the rate of O_2 diffusion was fierce enough so that the loose ZrO_2 shell cannot stop the O_2 to interact with the magnetic cores, which lead to the oxidation of the magnetic cores and the degradation of magnetic property. When we coat the cores with shells that are thick and compact (MA-3, 4, 5), the results shows a different trends, the value of μ' and μ'' of sample MA-3, 4, 5 decreases quite slightly with the increasing of temperature. At the temperature of 500 °C, the value of μ' and μ'' only decreased by 3.7% and 4.2% (MA-3), 4.2% and 3.9% (MA-4), 2.2% and 3.3% (MA-5). Conclusion can be drawn that the thick and compact ZrO_2 shells can effectively resist the diffusion of O_2, and protect the magnetic cores of the materials from being oxidized. The same rule holds for the rest part of the whole frequency of from 2 - 18GHz, such as 8 (Fig 7b), 13 (Fig 7d), and 18 GHz (Fig 7d).

Figure 7 The real part (μ') and imaginary part (μ'') of the complex permeability of MA1-5 at four typical frequencies 3GHz (a), 8 GHz (b), 13 GHz (c), 18 GHz(d) and three temperatures (20 °C, 250 °C, 500 °C)

The reflection loss (RL) values of the five microwave absorbers were calculated (Figure 8) using the relative complex permittivity and permeability at a given frequency and thickness layer according to the transmit line theory, which is summarized as the following equations.

$$Z_{in}=\sqrt{\mu r/\varepsilon r}\tanh[-j(2\pi fd/c)\sqrt{\mu r/\varepsilon r}]$$

$$RL(dB) = -20\lg_{10}|(Z_{in}-1)/(Z_{in}+1)|$$

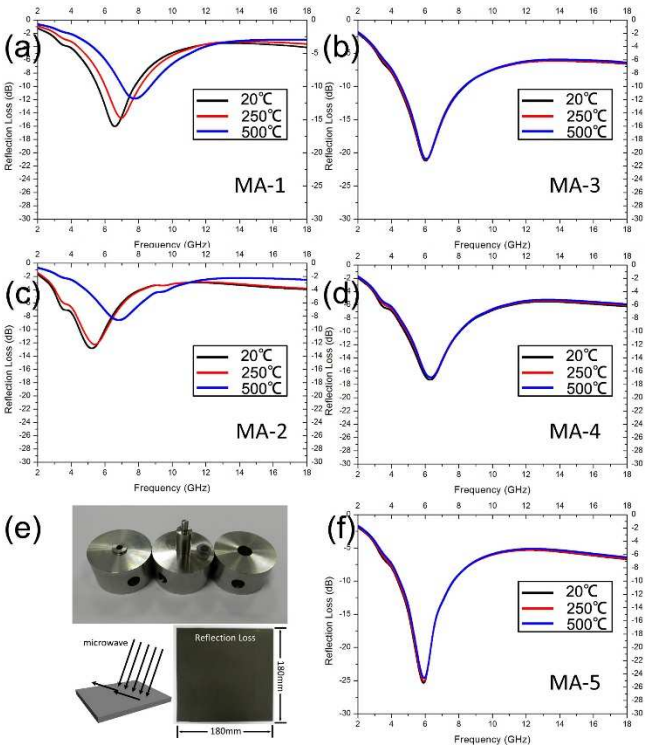

Figure 8 The reflection loss of MA-1(a), 2(c), 3(b), 4(d) and 5(f) at three temperatures 20 ºC, 250 ºC and 500 ºC. (e) The testing method of microwave absorption.

MA-1 exhibit various absorption performance measured at the three different temperatures. At 20°C, the MA-1 absorber has the largest absorption peak by -16.03 dB at the frequency of 6.6 GHz. However, with the temperature increasing, the largest absorption correspondingly decreased to -14.78 dB at the frequency of 7 GHz (250 °C) and -11.87 dB at the frequency of 7.8 GHz (500 °C) which is consistent with what we discussed above (Figure 8A). As for MA-2, only slight difference was found from the curves between 20°C and 250°C, however, higher temperature (500 °C) results in considerable decrease of reflection loss, and frequency corresponding to loss peak shift from 5.8 GHz to 7.2 GHz. This degradation of absorption capability measured from MA-1 and MA-2 could be attributed to the fact that no or insufficient shell thickness of ZrO_2 ceramic was coated outside MA-1 and MA-2, respectively, thus failed to provide enough protection under high-temperature. For

MA-3, MA-4 and MA-5, reflection loss show undistinguished dependency on the temperature. Based on a careful analysis of the reflection loss data at 500 °C, MA-3, MA-4 and MA-5 were regarded to have remarkable advantage over MA-1 and MA-2 in thermostable property. The main reasons and indications include: (1) enough thickness of ZrO_2 ceramic shell is essential to heat-resistance and anti-oxidation; (2) from RL data of MA-1 and MA-2, in which no enough anti-oxidation effect can be provided, complex permittivity and permeability of Fe_3O_4 core were inevitably degraded, thus leading to peak shifting and strength weakening of microwave absorption;

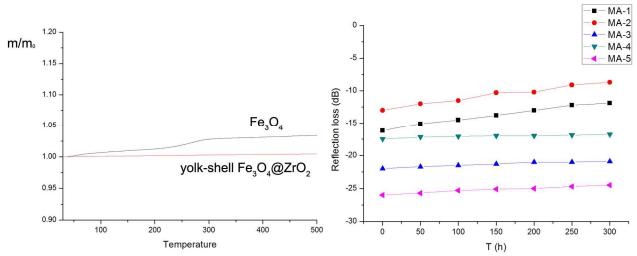

Figure 9 (a) the results of the thermogravimetric analysis of Fe_3O_4 and Fe_3O_4@ZrO_2, (b) the result of the analysis of microwave absorption property attenuation of the materials under high temperature over time.

The microwave absorption property attenuation of the materials under high temperature was evaluated by a characterization of the dependency of reflection loss on time. We recorded the largest reflection loss of each sample (MA-1-5) at 500 °C every 50 hours. As shown in figure 9, the reflection loss of MA-1 and 2 attenuate greatly over time, whereas the property of MA-3-5 didn't drop a lot. A thermogravimetric analysis of Fe_3O_4 and Fe_3O_4@ZrO_2 was carried out to evaluate the effect of ZrO_2 in protecting the internal magnetic core. The samples were exposed in air and heated to 500 °C at a rate of 10 K min^{-1}. The results revealed that Fe_3O_4 was oxidized into Fe_2O_3 quickly, since the weight of the sample increased by about 3%, which accord with the transformation of Fe_3O_4 to Fe_2O_3. However the weight of Fe_3O_4@ZrO_2 didn't increased a lot over time, indicating the composition of the material didn't change a lot over time.

Experimental

Materials:

Ferric chloride hexahydrate ($FeCl_3 \cdot 6H_2O$),ethylene glycol, sodium acetate, trisodiumcitrate, tetraethyl orthosilicate (TEOS), ethanol, ammonium hydroxide solution (28 wt %) Gold(III) chloride trihydrate(≥99.9% trace metals basis) were all purchased from Shanghai Sinopharm Chemical Reagent Co., Ltd. zirconium(IV) butoxide solution (80 wt.% in 1-butanol) (TBOZ), Hydroxypropyl cellulose (average Mw ~80,000) and Sodium borohydride($NaBH_4$) were obtained from Sigma-Aldrich. (3-Aminopropyl)triethoxysilane (≥ 98%) were obtained from Alfa-Aesar. All chemicals were of analytical grade and used without further purification. Deionized (DI) water obtained from Milli-Q system (Millipore, Bedford, MA) was used in all experiments.

Synthesis procedures

Preparation of Fe_3O_4 Particles: Fe_3O_4 nanoparticles were synthesized by a solvothermal process, 0.87 g $FeCl_3 \cdot 6H_2O$ (0.004 mol) and 0.1 g trisodiumcitrate were dissolved in 40 mL ethylene glycol (EG). Then a solution of 40 mL ethylene glycol containing 4 g NaAc were added to the former solution under magnetic stirring. The mixture was stirred vigorously for another 30 minutes before transferred into a Teflon-lined stainless-steel autoclave with a capacity of 100 mL. The autoclave was heated to 200 °C for 10 h, and then cooled to room temperature. At last, the product was rinsed with alcohol for 4 times and dried in 60 °C for 6 h.

Synthesis of Fe_3O_4@SiO_2 core-shell microspheres: 0.08 g as-prepared Fe_3O_4 particles were dispersed in the mixture of ethanol (160 ml) and DI water (38 ml) by ultrasonication. 2 mL of Ammonium hydroxide solution were added afterward. The solution was kept in ultrasonication for another 30 minutes. After that, the solution was transferred into a 500 ml boiling flask-3-neck under mechanical stirring. 0.2 ml TEOS were added to the solution dropwise, 0.6 mL more TEOS was added 30 minutes later. The reaction process was allowed to proceed for 3 hours under stirring. The product was dispersed in 40 mL ethanol to form a colloidal dispersion after being rinsed with ethanol for 4 times.

Synthesis of Fe_3O_4@SiO_2@ZrO_2 microspheres: 0.02 g Hydroxypropyl cellulous (HPC) was dissolved in a mixture of ethanol (98 mL) and DI water (0.5 mL). 10 mL the Fe_3O_4@SiO_2 colloidal dispersion was added into the former solution under mechanical stirring and kept for another 1 h. After that, the solution was transferred into a 250 ml boiling flask-3-neck. 1.72 mL zirconium (IV) butoxide solution was diluted with 20 mL ethanol, and then added to the flask dropwise in 5 minutes with a constant pressure dropping funnel. The reaction was carried out at room temperature overnight. Product was rinsed with ethanol for several times and dried at 60 °C for 6 h. The removal of the organics and crystallization of ZrO_2 were achieved by calcination in air by heating the product from room temperature to 500 °C at a rate of 2 K min^{-1}.

Synthesis of yolk-shell Fe_3O_4@ZrO_2 microspheres: As-prepared Fe_3O_4@SiO_2 @ZrO_2 microspheres were dispersed in 100 mL NaOH solution (0.5M) and heated at 60 °C under stirring for 12 h. The solution were then removed and replaced with 100mL new NaOH solution, mechanical stirring kept for another 24 h. The product were rinsed with DI water for 4 times and dried at 60 °C for 6 h. The calcination step was similar as the method mentioned above.

Characterization:

The size and morphology of the products were characterized by FESEM (Hitachi, S-4800) and TEM (JEOL, JEM-2100F). The samples for FESEM or TEM measurements were dispersed in ethanol and then dried on the silicon substrates or carbon-

coated copper grids, respectively. HRTEM, HAADF-STEM, EDS, were performed on the JEOL JEM-2100F transmission electron microscope equipped with a postcolumn Gatan imaging filter (GIF-Tridium) at an acceleration voltage of 200 kV. XRD measurements were acquired using a Bruker D8 X-ray diffractometer with Ni-filtered Cu Kα radiation (40 kV, 40 mA). Microwave absorption properties were studied by dispersing the samples into epoxy resin (EP) with a weight ratio of 1:5 according to the optimized proportion. A portion of the composite was coated on an aluminum substrate (180 mm × 180 mm) with a thickness of 2 mm to measure the reflection loss of the samples. The remaining sample was molded into the hollow pipe of a rectangular wave guide cavity with dimensions of 10.2 mm × 2.9 mm × 1.2 mm for complex permittivity and permeability measurements. The complex relative permittivity, permeability, and reflection loss were measured with a HP8510C vector network analyzer in the 2-18 GHz range. Heating equipment was used when the samples needed to be heated to the specific temperature.

Conclusions

In summary, we have demonstrated a HPC-assisted sol-gel method to synthesize yolk-shell Fe_3O_4@ZrO_2 microspheres. The mechanism of the reaction was proposed by pointing out the role of HPC played in controlling the sol-gel process as a dispersing reagent to disperse core/shell structures homogeneously in solution and a H_2O sustained-release agent to control the hydrolysis rate of zirconium precursor. ZrO_2 shelled magnetic core shows high temperature stability in microwave absorption property, as the reflection loss value of which didn't show distinguished decreasing under the temperature of 500 °C. Such results indicate that ZrO_2 coated microwave absorber may be an attractive candidate for high-temperature stable microwave absorbers.

Acknowledgements

This work was supported by the Ministry of Science and Technology of China (973 Project Nos. 2013CB932901 and 2009CB930803), and the National Natural Foundation of China (Nos. 51172047, 50872145, 51102050 and U1330118). Shanghai Pujiang Program and "Shu Guang" project of Shanghai Municipal Education Commission and Shanghai Education Development Foundation (09SG01) sponsored this research.

Notes and references

[a]2205 Songhu Road, Laboratory of Advanced Materials, Fudan University, Shanghai, 200438, China
[b]220 Handan Road, Department of Materials Science, Fudan University, Shanghai, 200433, China
[c]220 Handan Road, Department of Chemsitry, Fudan University, Shanghai, 200433, China

Electronic Supplementary Information (ESI) available: [The TEM images of the procedure in preparing Au nanoparticles implanted Fe_3O_4@SiO_2@ZrO_2 microspheres. Diagram of the frequency dependence of real and imaginary parts of complex permittivity and permeability of MA 1-5]. See DOI: 10.1039/b000000x/

1. J. Liu, S. Z. Qiao, J. S. Chen, X. W. Lou, X. Xing and G. Q. Lu, *Chemical Communications*, 2011, **47**, 12578-12591.
2. J. Liu, S. Z. Qiao, S. B. Hartono and G. Q. Lu, *Angewandte Chemie-International Edition*, 2010, **49**, 4981-4985.
3. C. Chen, X. Fang, B. Wu, L. Huang and N. Zheng, *Chemcatchem*, 2012, **4**, 1578-1586.
4. X. Fang, Z. Liu, M.-F. Hsieh, M. Chen, P. Liu, C. Chen and N. Zheng, *Acs Nano*, 2012, **6**, 4434-4444.
5. C.-H. Kuo, Y. Tang, L.-Y. Chou, B. T. Sneed, C. N. Brodsky, Z. Zhao and C.-K. Tsung, *J. Am. Chem. Soc.*, 2012, **134**, 14345-14348.
6. J. Gao, G. Liang, J. S. Cheung, Y. Pan, Y. Kuang, F. Zhao, B. Zhang, X. Zhang, E. X. Wu and B. Xu, *J. Am. Chem. Soc.*, 2008, **130**, 11828-11833.
7. G. Song, C. Li, J. Hu, R. Zou, K. Xu, L. Han, Q. Wang, J. Yang, Z. Chen, Z. Qin, K. Ruan and R. Hu, *Journal of Materials Chemistry*, 2012, **22**, 17011-17018.
8. Y. J. Hong, M. Y. Son and Y. C. Kang, *Advanced Materials*, 2013, **25**, 2279-2283.
9. J. Liu, Y. Zhou, J. Wang, Y. Pan and D. Xue, *Chemical Communications*, 2011, **47**, 10380-10382.
10. N. Liu, H. Wu, M. T. McDowell, Y. Yao, C. Wang and Y. Cui, *Nano Letters*, 2012, **12**, 3315-3321.
11. J. Liu, J. Cheng, R. Che, J. Xu, M. Liu and Z. Liu, *Acs Applied Materials & Interfaces*, 2013, **5**, 2503-2509.
12. J. Liu, J. Xu, R. Che, H. Chen, M. Liu and Z. Liu, *Chemistry-a European Journal*, 2013, **19**, 6746-6752.
13. J. Gao, G. Liang, B. Zhang, Y. Kuang, X. Zhang and B. Xu, *J. Am. Chem. Soc.*, 2007, **129**, 1428-1433.
14. F. Zhang, G. B. Braun, Y. Shi, Y. Zhang, X. Sun, N. O. Reich, D. Zhao and G. Stucky, *J. Am. Chem. Soc.*, 2010, **132**, 2850-+.
15. L. Zhang, T. Wang, L. Yang, C. Liu, C. Wang, H. Liu, Y. A. Wang and Z. Su, *Chemistry-a European Journal*, 2012, **18**, 12512-12521.
16. M. Goswami, A. Patil and G. P. Kothiyal, in *Solid State Physics, Vol 57*, eds. A. K. Chauhan, C. Murli and S. C. Gadkari, Amer Inst Physics, Melville, 2013, pp. 548-549.
17. H. Tsukamoto, Y. Komiya, H. Sato and Y. Watanabe, in *Fourth International Conference on Smart Materials and Nanotechnology in Engineering*, eds. J. A. Epaarachchi, A. K. T. Lau and J. Leng, Spie-Int Soc Optical Engineering, Bellingham, 2013.
18. M. P. Gashti and A. Almasian, *Composites Part B-Engineering*, 2013, **52**, 340-349.
19. P. M. Arnal, M. Comotti and F. Schueth, *Angewandte Chemie-International Edition*, 2006, **45**, 8224-8227.
20. P. M. Arnal, C. Weidenthaler and F. Schuth, *Chem. Mat.*, 2006, **18**, 2733-2739.
21. A. Dokoutchaev, J. T. James, S. C. Koene, S. Pathak, G. K. S. Prakash and M. E. Thompson, *Chem. Mat.*, 1999, **11**, 2389-2399.
22. A. G. Dong, N. Ren, Y. Tang, Y. J. Wang, Y. H. Zhang, W. M. Hua and Z. Gao, *J. Am. Chem. Soc.*, 2003, **125**, 4976-4977.
23. Y. Q. Jiang, S. F. Yang, X. F. Ding, Y. P. Guo, H. Bala, J. Z. Zhao, K. F. Yu and Z. C. Wang, *Journal of Materials Chemistry*, 2005, **15**, 2041-2046.
24. Y. D. Xia and R. Mokaya, *Journal of Materials Chemistry*, 2005, **15**, 3126-3131.

25. J. L. Yin, X. F. Qian, H. Yin, M. W. Shi, H. C. Zhang and G. T. Zhou, *Inorganic Chemistry Communications*, 2003, **6**, 942-945.
26. N. Kawahashi, C. Persson and E. Matijevic, *Journal of Materials Chemistry*, 1991, **1**, 577-582.
27. J. M. Kim, S. M. Chang, S. Kim, K.-S. Kim, J. Kim and W.-S. Kim, *Ceramics International*, 2009, **35**, 1243-1247.
28. L. M. Liz-Marzan, M. Giersig and P. Mulvaney, *Langmuir*, 1996, **12**, 4329-4335.
29. A. Lombardi, M. P. Grzelczak, A. Crut, P. Maioli, I. Pastoriza-Santos, L. M. Liz-Marzan, N. Del Fatti and F. Vallee, *Acs Nano*, 2013, **7**, 2522-2531.
30. P. Reineck, D. Gomez, S. H. Ng, M. Karg, T. Bell, P. Mulvaney and U. Bach, *Acs Nano*, 2013, **7**, 6636-6648.
31. W. Li, J. Yang, Z. Wu, J. Wang, B. Li, S. Feng, Y. Deng, F. Zhang and D. Zhao, *J. Am. Chem. Soc.*, 2012, **134**, 11864-11867.
32. W. F. Ma, Y. Zhang, L. L. Li, L. J. You, P. Zhang, Y. T. Zhang, J. M. Li, M. Yu, J. Guo, H. J. Lu and C. C. Wang, *Acs Nano*, 2012, **6**, 3179-3188.
33. H. Sakai, T. Kanda, H. Shibata, T. Ohkubo and M. Abe, *J. Am. Chem. Soc.*, 2006, **128**, 4944-4945.
34. D.-D. Zhang, D.-L. Zhao, J.-M. Zhang and L.-Z. Bai, *Journal of Alloys and Compounds*, 2014, **589**, 378-383.
35. J. Zheng, H. Lv, X. Lin, G. Ji, X. Li and Y. Du, *Journal of Alloys and Compounds*, 2014, **589**, 174-181.
36. J. Liu, R. Che, H. Chen, F. Zhang, F. Xia, Q. Wu and M. Wang, *Small*, 2012, **8**, 1214-1221.
37. J. Liu, J. Cheng, R. Che, J. Xu, M. Liu and Z. Liu, *Journal of Physical Chemistry C*, 2013, **117**, 489-495.
38. J. Liu, J. Xu, R. Che, H. Chen, Z. Liu and F. Xia, *Journal of Materials Chemistry*, 2012, **22**, 9277-9284.
39. W. Duan, X. Yin, Q. Li, X. Liu, L. Cheng and L. Zhang, *Journal of the European Ceramic Society*, 2014, **34**, 257-266.
40. Q. Li, X. Yin, W. Duan, B. Hao, L. Kong and X. Liu, *Journal of the European Ceramic Society*, 2014, **34**, 589-598.
41. Y. Shi, F. Luo, D. Ding, J. Gui, W. Zhou and D. Zhu, *Physica Status Solidi a-Applications and Materials Science*, 2013, **210**, 2668-2673.
42. F. Ye, L. Zhang, X. Yin, Y. Zhang, L. Kong, Y. Liu and L. Cheng, *Journal of the European Ceramic Society*, 2014, **34**, 205-215.

Table of Content